University of Liverpool

MATH 552: Preliminary Dissertation

Vertex Dynamical Model

Author:
Nor Zubaidah Hassan

Supervisor:
Dr. Bakhti Vasiev

September 12, 2012

Contents

1 Introduction

Tissues in living organisms are made up of cells. These cells grow, divide and move. Some cells produce chemicals and some move against or along a chemical gradient (chemotaxis). In response to these chemicals, the cells can change shape. Studying and analysing these behaviour of cells in tissues are the area of interest for biologist as well as physicist and mathematicians. They are interested in discovering how cells move, proliferate and change their shapes. In tissue development, cell rearrangement is an important process driving epithelial morphogenesis in the many development settings. Various mechanical models provide insight into the dynamics of cells rearrangement within an epithelial sheet and numerical simulations carried out in the models can reproduce the essential features of cell shape change and cell rearrangement observed during normal development.

Boundary dynamics model such as Cellular Potts model and 2 or 3-D vertex dynamics model are usually used in studying the dynamics of cell rearrangement, deformation as well as proliferation. The idea behind these models are to describe cell rearrangement by accounting for the balances of forces between neighbouring cells within an epithelium. Cell rearrangement and cell shape changes i.e. deformation occur when these forces are not in mechanical equilibrium.

In the Cellular Potts model which is then called the Glazier - Graner - Hogeweg model (GGHM) as it was originally developed by Graner and Glazier, each cell is represented by a number of grid points on a regular lattice. So when the cell moves, it either loses or gain some grid points on the lattice. The model describes cell patterns by the shape of their boundaries (many lattice points along boundaries). It does not make an assumption about edge and face shapes. Curved faces and edges could appear during simulations. The original implementation of GGHM was based on the *Monte Carlo algorithm*. At each time step, the probability, p, to change the state for all grid points are calculated using the *Bolzmann function*, $p = -e^{-\frac{\nabla E}{T}}$ where T is temperature and E is energy defined in such a way that it accounts for the work done by different forces acting upon moving or deforming cells. For each grid point, a neighbour is selected randomly and we calculate how the energy of the system will change after changing the state of the grid point to that of its neighbour. If change results in energy decrease, then we allow the change to occur. Else, we calculate the probability of the change. i.e. p. The different forces taken into account for the calculation of energy, E, are the adhesive forces between cells, force associated with the incompressibility of cells (pressure) and forces developed by chemotactically (against chemical gradient) moving cells. i.e.

$$E = E_{\text{adhesive}} + E_{\text{pressure}} + E_{\text{chemotaxis}} \,.$$

This model is robust. Small variations in the values of model parameters do not alter quantitatively the outcome of simulations.

As for the vertex model, before it was introduced, Weliky and Oster [1] wrote an article about a mechanical model for cell rearrangement. In their paper, cells are treated as 2-D polygons where mechanical forces are applied to the polygonal vertices. The epithelial sheet is modelled by allowing adjacent cells to share common boundary vertices (Figure 1). A single vertex may experience forces generated by more than one cell. In addition to forces generated by cells, external vector forces can be applied to particular common boundary vertices if necessary. This allows the model to simulate stretching and deformation of the cell sheet by forces extrinsic to the epithelium.

The total vector force acting on such a vertex is simply the sum of all forces from the cells sharing this vertex plus the external forces. When vertex tensions and pressures are in mechanical equilibrium, the vertex position will not change. However, unbalanced forces can result in cell protrusion and subsequent cell rearrangement, which occur when 2 vertices meet.

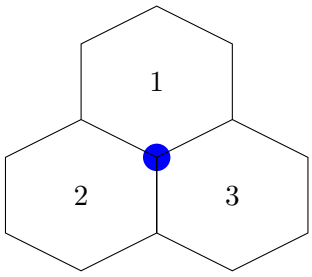

Figure 1: Adjacent cells sharing common junctional vertex.

For my paper, I will be describing the vertex dynamical model and it's application to the study of the dorsal-ventral organizer of the imaginal wing disc of the Drosophila.

2 Original Vertex Model developed in [2] (3D-model)

In this section, I give an overview of the article by Nagai, Tanemura and Honda.

A cell aggregate, when subjected to mechanical deformation, relaxes as elastic materials on short-time scale and as viscous liquids on long time scale. In other words, a cell deformed under the short-time influence of force will return to its original shape but will not do so if the force is applied for a long period of time.

To investigate the cell shape, deformation and rearrangement of cells under the influence of external force in 3D multicellular aggregates, the 3D vertex model which provides the vertex positions of cells and the shapes of cell surfaces in a cell aggregate is developed. The model was confirmed to simulate behaviours of cells, minimizing the cell interface areas. It also provides an additional insight into the role of cell mechanical properties in the behaviour of viscoelastic tissues.

We consider a tissue consisting of many cells to be a 3D space tessellation, which consists of convex polyhedra without gaps or overlaps. Since a topologically stable random cellular structures are considered, a **vertex** in 3D space generally connects to 4 neighbouring vertices by 4 edges. 3D space tessellation pattern consisting of faces instead of edges are considered as we treat a cell aggregate as consisting of cell membranes, not of atoms and bonds in amorphous materials.

In the 3D vertex model, we look at the interfaces between neighbouring cells and volumes of polyhedral cells which are represented by vertices. These interfaces and volumes have to be expressed by vertex coordinates. As such, we have that the vertices obey the equation of motion:

$$\eta \frac{dr_i}{dt} = -\nabla_i U \,, \tag{1}$$

$(i = 1, \ldots, n_v)$.

i refers to the vertex where n_v is the total number of vertices of the cell aggregate.

The term on the **left-hand side** of equation (1) represents the viscous drag:

- η : friction between the vertices. It is a positive constant based on the assumption that the circumference around vertex i does not extremely differ from each other. It comes from the energy dissipation associated with interface motion.

- r_i : a 3-dimensional position vector of vertex i. Therefore $\frac{dr_i}{dt}$ is the velocity of the vertex.

The term on the **right-hand side** of equation (1) represents forces acting upon the vertex:

∇_i : vector differential operator

U : potential (free energy) which includes various terms related to cell surface area, cell volume and potential energy due to external forces, expressed in terms of vertex coordinates.

$\nabla_i U$: potential/driving force, which is minus the gradient of the potential U.

Aside: Equation (1) is derived from the *Navier-Stokes* equation [10]:

$$F = ma = -\mu\nabla V_1 + f_{\text{friction}} + f_{\text{interface}} + f_{\text{pressure}} + \cdots$$

where $\mu\nabla V_1$ represent the viscosity and f is force. Although we have cells around the fluid, it is the cells, not the fluid that are moving. Therefore $\mu\nabla V_1 = 0$. Furthermore we neglect inertia. i.e. $ma = 0$.

We then replace each of the force by the minus of the gradient of the potential, except for friction. We have $f_{\text{friction}} = -\eta V_i$.

$$\begin{aligned} \eta V_i &= -\nabla U_{\text{interface}} - \nabla U_{\text{pressure}} + \cdots \\ &\Rightarrow \eta \tfrac{dr_i}{dt} = -\nabla_i U. \end{aligned}$$

U will take into account all forces. We will consider two of them, represented by U_s which accounts for the surface tension and U_v which accounts for incompressibility. U_s is given by the equation:

$$U_s = \sigma \sum_f S_f + \sigma_0 \sum_m S_m \,, \tag{2}$$

$(f = 1, 2, \ldots, n_f \quad ; \quad m = 1, 2, \ldots, n_m)$,

where

S_f : surface area of polygon f facing adjacent cells

σ : interface energy per unit area

S_m : surface area of polygon m facing the external culture medium

σ_0 : surface energy per unit area

n_f, n_m : number of polygons facing an adjacent cell and external culture medium respectively.

S_f and σ represent the interface energy between neighbouring cells while S_m and σ_0 represent the surface energy between cells and the external culture medium. S_f and S_m can be computed by the triangulation of polygons. In cell aggregates without external culture medium (i.e. with periodic boundary conditions), equation (2) will not have the 2$^{\text{nd}}$ term, $\sigma_0 \sum_m S_m$.

U_v which gives the cell volume constraint is given by the equation

$$U_v = \kappa \sum_{\alpha} (V_\alpha - V_{std})^2 \,, \tag{3}$$

$(\alpha = 1, 2, \ldots, n)$,

where

κ : positive constant

n : total number of cells

V_α : volume of cell α

V_{std} : volume of relaxed cells, defined as the average volume of all cells.

Equations (2) and (3) are transformed using new dimensionless quantities r'_i, $\nabla'_i (= \frac{\partial}{\partial r'_i}), S'_f, S'_m, V'_\alpha$ and V'_{std} as follows:

$$r_i = r'_i R_0, \nabla_i = \nabla'_i / R_0, S_f = S'_f R_0^2, S_m = S'_m R_0^2, V_\alpha = V'_\alpha R_0^3, V_{std} = V'_{std} R_0^3. \tag{4}$$

After the transformation using equation (4), we get the **equation of motion for the cell aggregate (without centrifugation)**, to be

$$\frac{dr'_i}{dt'} = -\nabla'_i \left\{ \sum_f S'_f + \sigma_0 \sum_m S'_m + \kappa' \sum_\alpha (V'_\alpha - V'_{std})^2 \right\}, \tag{5}$$

where

$$t' = t\sigma/\eta, \sigma'_0 = \sigma_0/\sigma, \kappa' = R_0^4 \kappa/\sigma \,.$$

and omitting the primes ($'$), we get

$$\frac{dr_i}{dt} = -\nabla_i \left\{ \sum_f S_f + \sigma_0 \sum_m S_m + \kappa \sum_\alpha (V_\alpha - 1)^2 \right\}. \tag{6}$$

If we would like to describe the experiment of flattening a cell aggregate under centrifugal force or gravity, we will then have 2 additional terms, U_z and U_{floor}. Refer to Appendix A.1 for details on these 2 terms.

Further, equation (1) expresses completely dissipative vertex motion under the potential U. Differentiation of the potential U with respect to time gives the inequality

$$\frac{dU}{dt} = \sum_i \frac{dr_i}{dt} \nabla_i U = -\eta \sum_i (\frac{dr_i}{dt})^2 \ \leq 0. \tag{7}$$

This inequality indicates that U decreases during motion. For example, if U is the total surface area of cell boundaries, the vertices move to reduce the total surface area. Also, equation (7) is deterministic. The vertices follow the gradient of the position-dependent energy, so the cells passively change their shape to satisfy equation (7).

We also define the degree of **flatness** of a polyhedron in the z-direction with the following equation

$$\frac{\sum_i \left\{ (x_i - x_G)^2 + (y_i - y_G)^2 \right\}}{\sum_i (z_i - z_G)^2}, \tag{8}$$

where (x_G, y_G, z_G) is the center of mass of the polyhedron and summations are over all polyhedron vertices. Flatness is sensitive to the shape of the polyhedron, because for flatter polyhedra, the denominator of equation (8) becomes small. Flatness does not diverge since polyhedra cells always have finite volumes in the simulations.

In addition to the equations of motion, the model also involves an elementary process of reconnection of neighbouring vertices. Vertex dynamics including vertex reconnection is important as it can reduce the interface energy of cells. Also, if no reconnection is involve, then the evolving pattern according to equation (1) preserves its initial topology, which is not the case of interest.

When the length of an edge connecting two neighbouring vertices is short (say, less than a critical δ), the neighbours reconnect and the neighbour relationships of the vertices changes. The steps to perform the reconnection are as follows:

Step 1 : All edge lengths are calculated and an ascending list for the length of edges shorter than the critical length δ are made.

Step 2 : (i) Edges ij are picked sequentially from the list of short edges.

(ii) If the vertex i or j connects to edges that have already reconnected, then the edge is skipped.

(iii) Steps (i) and (ii) are then repeated for the next edge in the list.

(iv) Otherwise, the number of triangles the edge belongs to are counted.

In general, each edge belongs to 3 polygons. If none or one of the polygons are triangles, we proceed with the reconnection. However, if 2 or more of the polygons are triangles, we skip the edge and repeat Step 2. When all the edges in the list have been reconnected, the step ends.

For the reconnection, we do not consider any flunctuations in cell movement coming from thermal noise or from active cell motility through the consumption of metabolic energy.

In a nutshell, the 3D vertex dynamics model explicitly showed that cell movement in a 3D cell aggregate is possible. The cell movement belongs to slippage resulting in rearrangement of neighbouring cells. Surface minimization by cells helps to drive cell movement and influences the properties of the cell aggregate. The model also provides vertex positions and boundary faces, and is convenient to visually present polyhedral cell shapes. The model has a characteristic time scale $\frac{\eta}{\sigma}$ which contains 2 material constants. The coefficient η (friction) and σ (interfacial tension) can be determined independently by dynamics and static measurement, respectively. When experiments provide these material constants, the vertex dynamics specify a time-scale by which it can be tested.

3 Modified Vertex Model developed in [3] (2D-model)

In this section, I give an overview of the article by Farhadifar, Röper, Aigouy, Eaton and Jülicher.

An epithelia is made up of cells that are packed together, forming cell junctions which come into contact with one another. It is important for the cells to regulate intercellular junctional networks for tissue formation and function. Junction remodelling underlies many of the dramatic tissue reorganisation occurring during development. This tissue rearrangement then allows the development of the specific packing geometries of the epithelia, which is a consequence of both the physical properties of the cells and the disordering influence of proliferation.

For the 3D model in the previous section, we looked at the effect of pressure on the rearrangement and deformation of cells. In the 2D model to be described in this section, we will also be looking at how cellular properties and cell proliferation cause the rearrangement of cells.

We are interested in studying the epithelial cell-packing in the larval wing disc of the Drosophila. During the larval stage, tissue proliferates rapidly, causing a geometric disorder induced by cell division in proliferating epithelia. There is molecular machinery that reorganises epithelial contacts. The molecules alter the cell-packing by changing force balances within the epithelium. The molecule E-Cadherin mediates adhesion between adjacent cells but also organises a subcortical actin-myosin cytoskeleton. In other words, it binds cells to other cells. (Actin-myosin are proteins where the regulation of its contractility can alter the structure of the junctional network and is thought to contribute to the morphogenic movements in epithelial cells).

Cells are represented as polygons with cell edges defined as straight lines connecting vertices.(This is a good approximation for the wing disc epithelium). For a cell-packing, getting a hexagonal packing is favoured because of its advantages. It minimizes light scattering by plasma membranes and hexagonally packed hairs on the surface of the Drosophila wing guide airflow during flight. Further, in the Drosophila wing epithelium, cells convert from an irregular to hexagonal array shortly before hair formation. However, less than half of the cells that proliferates were hexagonal. Most cells are irregularly packed. As such, reorganization or remodelling of the epithelial contacts to form hexagonal array is important. We will discuss more on the Drosophila wing in the next section. For this section, I will explain the details of the 2D model.

To understand remodelling, one must develop a physical description of the epithelium that can account for rearrangement of the junctional network. During cell proliferation and cell division, cells with different neighbour numbers are present in

reproducible proportion. The redistribution of neighbours after cell division depends on the physical properties of the cells. To illustrate packing geometries of apical junctions based on the physical properties of cells (as it redistribute the neighbours), the 2D vertex model was developed which describes the forces that acts to displace the vertices of the polygons.

In the model, cell packings correspond to stable and stationary network configurations obtained by minimization of a potential function. This approach is used to study the role of cell mechanics and cell division in determining network mechanics.

Further, we have N_c polygonal cells numbered by $\alpha = 1 \dots N_c$ and N_v vertices, numbered $i = 1 \dots N_v$ at which cell edges meet. The stable and stationary network configuration obeys a force balance which implies that the net force F_i acting on each vertex vanishes for all vertices. This means that the force at each vertex does not dissipate. It is local and independent. Hence at each vertex, the force vanishes, not transferred to another vertex. The forces considered can be represented by the energy function $E(R_i)$. Any stable and stationary configuration of the network then corresponds to a local minimum of the energy function. We have the following expression for $E(R_i)$:

$$E(R_i) = \sum_{\alpha} \frac{K_\alpha}{2}(A_\alpha - A_\alpha^{(0)})^2 + \sum_{<i.j>} \Lambda_{ij} l_{ij} + \sum_{\alpha} \frac{\Gamma_\alpha}{2} L_\alpha^2 \,. \tag{9}$$

Here $F_i = -\frac{\partial E}{\partial R_i}$.

This vertex model is different from the ones used before because it only represents the network of apical junctions and a quadratic perimeter energy is used.

$E(R_i)$ is made up of 3 forces due to **cell elasticity** (pressure and incompressibility), **actin-myosin bundles** (tension along edges) and **adhesion molecule** (perimeter tension).

The 1$^{\text{st}}$ term of equation (9), $\sum_\alpha \frac{K_\alpha}{2}(A_\alpha - A_\alpha^{(0)})^2$ describes **area elasticity** where

K_α : elastic coefficient

A_α : area of cell α

$A_\alpha^{(0)}$: preferred area determined by cell height and volume.

Here, the cell volume is assumed to be constant. If the cross-sectional area of the cell at the junctional levels is altered, there will be deformation of the cell in 3 di-

mension. Actually, as this model is 2 dimensional, we do not consider the cell height. We are looking at a single layer of the epithelia and the thickness (i.e. the height) of the epithelia is ignored. However, the area elasticity term in the energy function indirectly takes into account the cell height.

For the 2nd term of $E(R_i)$, Λ_{ij} represents the **line tensions** at junctions between individual cells. It describes forces resulting from cell-cell interactions along the junctional regions of specific cell boundaries. For example, it can be influenced by multiple mechanisms. It can be reduced by increasing cell-cell adhesion or reducing actin-myosin contractility. l_{ij} is the **length of the junction linking vertices i and j** and the sum over $< ij >$ is over all bonds.

As the length of the cell boundary l_{ij} between 2 vertices i and j increases, this term in the energy function decreases if Λ_{ij} is negative and increases if Λ_{ij} is positive.

The last term in the energy function is $\sum_\alpha \frac{\Gamma_\alpha}{2} L_\alpha^2$. Here, we are looking at the contractility of the actin-myosin which cause the perimeter of each cell to be reduced, thus affecting the line tension Λ_{ij} of the 2nd term. It also generates the coefficient Γ_α which describes the dependence of contractile tension on cell perimeter L_α. This contractility term involves the whole cell perimeter and is motivated by the fact that the actin-myosin ring appears to span the cell.

When the 2nd and 3rd terms tend to 0, we go towards minimization of energy (which is what we want). The 1st term will not be affected. If all the terms are 0, then all cells will collapse. However this is impossible since $A^{(0)}$ is non-zero. Therefore the 1st term of equation (9) is indeed important (we assume volume is constant).

Next, an important feature of this model is that it is in the ground state or most relaxed network configuration (also called global energy minimum). Although it is not realistic, it is important for reference.

In Figure 2, the ground state exists as a function of the parameters, line tension and contractility. It is determined by $\bar{\Gamma} = \Gamma / K A^{(0)}$, the **normalised contractility** and $\bar{\Lambda} = \Lambda / K (A^{(0)})^{3/2}$, the **normalised line tension**. We normalised Λ and Γ so that we can compare the 2nd and 3rd terms with the 1st term respectively. If $\bar{\Gamma}$ is small, then $\Gamma < K A^{(0)}$ (the area elasticity). The parameters ($\bar{\Lambda}$ and $\bar{\Gamma}$) are varied to disturb the stable and stationary network configurations which are affected by the local perturbations (cell division and slow changes in cell properties).

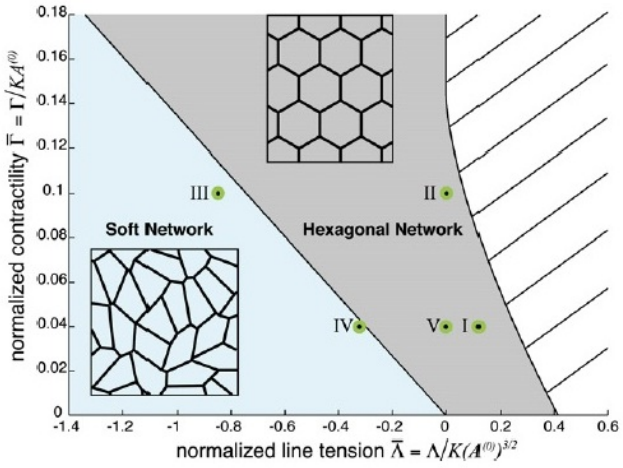

Figure 2: Ground-State Diagram
Diagram of the ground states of the energy function $E(R_i)$ as a function of the normalized line tension $\bar{\Lambda}$ and contractility $\bar{\Gamma}$. In the gray region, the ground state is a hexagonal network. In the blue region, the ground states are irregular soft networks and many configurations coexist. In the striped region to the right, where $\bar{\Lambda}$ is large, cell areas vanish and the model breaks down. Green dots indicate the parameter values for the different cases.

In this ground state, we can have 2 regions of network: the **hexagonal** (gray region of Figure 2) and **soft** network (blue region of Figure 2) where many configurations coexist. The hexagonal network corresponds to $\bar{\Lambda} < 0$ where the cell boundaries expand while the soft network corresponds to $\bar{\Lambda} > 0$ where the cell boundaries shrink.

For the hexagonal network, we have regular packing of cells. It is also called the single ground state. The constraint for this network is that all the edges of the polygons are the same. As such, the cells are unable to move. Both bulk and shear modulus are present and the cells are able to resist uniform compression (bulk modulus measures this). The cells also resist the shear force, allowing them to go back to their positions. These compression/expansion and shearing requires work to be done. This network is elastic and is analogous to the solid state.

On the other hand, the soft network has irregular packing of cells. In this network, the area and perimeter of the cells are the same. It allows cells to move past one another easily and can be sheared. Some cells will try to have a longer side than the others. As many packing geometries have the same minimal energy, this ground state is degenerate. As a result, the configuration can be sheared without any work required and has a vanishing shear modulus. For the packing geometries, the area of the cells are equal to the preferred area and their perimeter is given by $L_0 = -\Lambda/2\Gamma$. This region is analogous to the viscous or liquid state and can be easily remodeled.

Steps to obtain the dimensionless/normalised form to equation (9)

$$\begin{aligned} E(R_i) &= \sum_\alpha \frac{K_\alpha}{2}(A_\alpha - A_\alpha^{(0)})^2 + \sum_{<i.j>} \Lambda_{ij} l_{ij} + \sum_\alpha \frac{\Gamma_\alpha}{2} L_\alpha^2 \\ &= \sum_\alpha \frac{K_\alpha (A_\alpha^{(0)})^2}{2}(\frac{A_\alpha}{A_\alpha^{(0)}} - 1)^2 + \sum_{<i.j>} \frac{\Lambda_{ij}(A_\alpha^{(0)})^2}{(A_\alpha^{(0)})^{\frac{3}{2}}} \frac{l_{ij}}{\sqrt{A_\alpha^{(0)}}} + \sum_\alpha \frac{\Gamma_\alpha (A_\alpha^{(0)})^2}{2(A_\alpha^{(0)})} \frac{L_\alpha^2}{A_\alpha^{(0)}} \,. \end{aligned} \tag{10}$$

Dividing throughout by $K_\alpha (A_\alpha^{(0)})^2$, we obtain the dimensionless equation

$$\frac{E(R_i)}{K_\alpha (A_\alpha^{(0)})^2} = \sum_\alpha \frac{1}{2}(\frac{A_\alpha}{A_\alpha^{(0)}} - 1)^2 + \sum_{<i.j>} \frac{\Lambda_{ij}}{K_\alpha (A_\alpha^{(0)})^{\frac{3}{2}}} \frac{l_{ij}}{\sqrt{A_\alpha^{(0)}}} + \sum_\alpha \frac{\Gamma_\alpha}{K_\alpha (A_\alpha^{(0)})} \frac{L_\alpha^2}{2A_\alpha^{(0)}} \,. \tag{11}$$

We then define

$$\bar{\Lambda}_{ij} = \frac{\Lambda_{ij}}{K_\alpha (A_\alpha^{(0)})^{\frac{3}{2}}} \quad , \quad \bar{\Gamma}_\alpha = \frac{\Gamma_\alpha}{K_\alpha A_\alpha^{(0)}} \,. \tag{12}$$

When cell proliferates, they divide, bringing about rearrangement of cells. A standard algorithm is used in dividing a randomly selected cell. The steps involve in the algorithm are as follows: (refer to Figure 3 for pictorial description)

(1) Double the preferred area of cell.

(2) Divide the cells by introducing vertices generated by a new edge that is formed at a random angle and passes through the cell center, defined as the average of the vertex positions of the original cell.

(3) The 2 daughter cells are then assigned the parameter of the other cells, including the preferred area $A^{(0)}$.

(4) Resulting configuration is then again relaxed to the nearest stable state. During relaxation, edges might shrink or vanish if this leads to a further lowering of the energy. This can be followed by T1 or T2 transition.

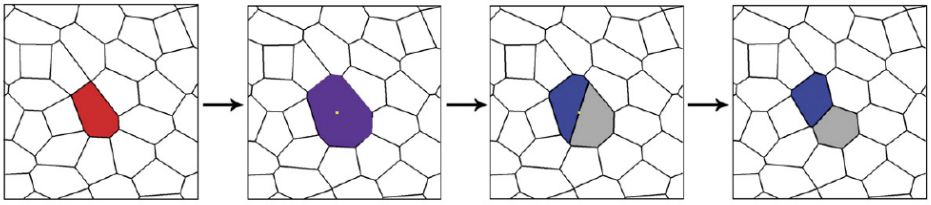

Figure 3: Cell Division in Vertex Model

For T1 process, the bond length between two 3-way vertices first shrinks to zero and subsequently expands in the opposite direction. This causes local changes in neighbour numbers of surrounding cells (cells which initially have no common boundary now do have it). Topology of the network is changed. For a T2 process, if the area of a triangle drops to zero, then it is replaced by a vertex. i.e. the cell is eliminated from the epithelium.

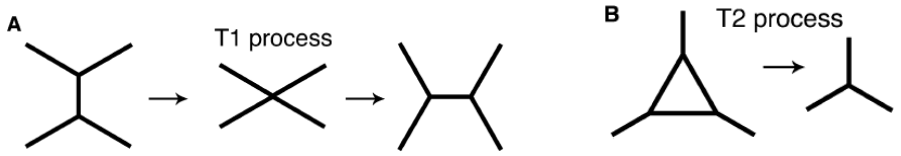

Figure 4: T1 and T2 process

After cells divide and relaxed, the network obtained may or may not be hexagonal. As mentioned earlier, hexagonal network has its advantages. To have a higher chance of obtaining such a network, we need to control the strength of fluctuations in adhesion and contractility of individual cell boundaries. For equation (9), we assume $l_{ij}^{(0)}$ and $L_\alpha^{2\,(0)}$ are zero. If they are non-zero, equation (9) will be

$$E(R_i) = \sum_\alpha \frac{K_\alpha}{2}(A_\alpha - A_\alpha^{(0)})^2 + \sum_{<i.j>} \Lambda_{ij}(l_{ij} - l_{ij}^{(0)}) + \sum_\alpha \frac{\Gamma_\alpha}{2}(L_\alpha^2 - L_\alpha^{2\,(0)}),$$

giving us more options to obtain a hexagonal network when we vary the parameters $\bar{\Gamma}$ and $\bar{\Lambda}$.

Proliferation is then simulated numerically to generate different network morphologies/structures that depend on physical parameters. These network differ in:

(1) polygon class distribution,

(2) cell area variation,

(3) rate of T1 and T2 transition during network growth.

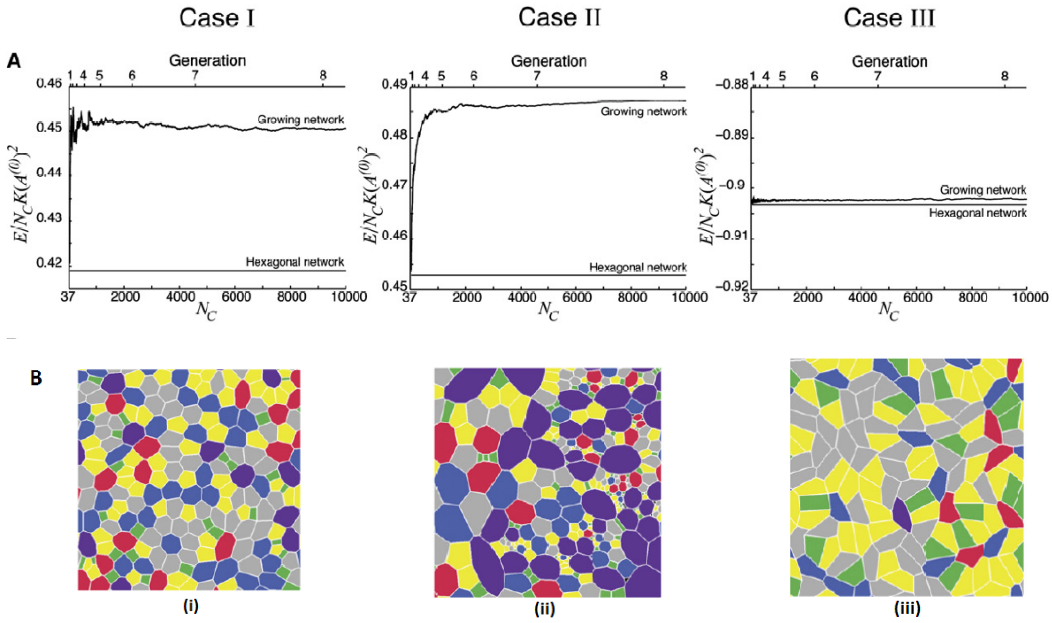

Figure 5: **A**: Energy per cell normalized by the reference elastic energy $K(A^{(0)})^2$ as a function of cell number N_c in simulations of network growth for the 3 cases, I, II, III, indicated in Figure 2. The generation number and energy of the corresponding hexagonal network are indicated. **B**: (i), (ii), (iii) are examples of stationary network patterns generated by repeated cell division for Cases I, II, III. Colour codes are used for the different polygon class.

Refering to Figure 5, for Case I indicated in the gray region of Figure 2, the energy per cell ($\frac{E}{N_C K(A^{(0)})^2}$) increases with increasing cell number (N_C) and then fluctuates around a constant value greater than the ground state value of the hexagonal lattice. For this case, $\bar{\Gamma} = 0.04$ and $\bar{\Lambda} = 0.12$. Case II ($\bar{\Gamma} = 0.1$ and $\bar{\Lambda} = 0.0$) is similar to Case I but the stationary network contains a smaller fraction of hexagonal cells compared to Case I. For Case III ($\bar{\Gamma} = 0.1$ and $\bar{\Lambda} = -0.85$), energy does not increase when the cells divide. Cells does not depend on neighbour number. In Case III of

Figure 5A, the small energy difference between ground state and simulation is due to numerical errors.

In a nutshell, to investigate the contributions of cell mechanics, adhesion and cortical contractility to the development of specific packing geometries, the 2D vertex model was developed for the junctional network. Configurations of the junctional network observed in tissues corresponds to network configurations for which forces are balanced. The model takes into account area elasticity of cells, line tension, contractility as well as perimeter of the cell. The important feature of this network is that it has 2 different types of relaxed network configurations which corresponds to global minima of energy function; the regular hexagonal network and irregular soft network. Further, varying the parameter values in the simulations shows that cell proliferation and physical properties of cells cause the rearrangement and packing disorder of the cells.

4 Further extension of the 2D Vertex Model developed in [4]

In this section, I give an overview of the article by Xandri, Sagués, Casademunt and Buceta.

4.1 The Biology: Drosophila Wing Epithelium

In the wing imaginal disc, a selector gene called apterous supply cells with a dorsal (front) character. This gene grant some properties that determine cellular interactions that in turn restrict their locations. e.g. affinity and adhesion. Thus cells under control of selector genes cannot intermingle freely and their positions become restricted to regions within the primordium: the so called **compartments**. The concept of compartment implies the existence of non-trivial boundaries that control cell migration.

Cellular population becomes specified by the boundary defining the so called **organizer**. An organizer acts in practice as the coordinate axis of a reference system. The organizer grows in one dimension since its thickness (width) remains constant, as opposed to the whole disc that grows isotropically in 2 dimensions. Many aspects of the Dorsal-Ventral (DV) organizer of the wing imaginal disc still remain puzzling. In particular, how this pattern can be progressively and robustly scaled as cell proliferation advances remains a riddle. Due to this, an in silico framework (performed on computer via computer simulation) that sheds light into the dynamics that shape the DV organizer for being an effective source of positional information and a cellular lineage controller is used. This approach introduces a realistic and novel description of the cellular dynamics of the DV organizer and neighbouring compartments, leading to a series of quantitative predictions that can be experimentally tested.

In the wing imaginal disc, the DV organizer (Figure 6) is located at both sides of the boundary. This has important implications with respect to the organizers characteristics and their role. The boundary is formed at the interface of two compartments. The DV boundary develops embedded within the DV organizer population and the entity that keeps cells segregated from opposite compartments is the organizer itself rather than the boundary. In other words, the dorsal and ventral cell populations are kept segregated by a cellular structure, namely the DV organizer. Using a fluid simile, we can say that in a 2 fluids mixture, it would be comparable to a fluid film that intercalates between them.

Further it has been suggested that the symmetrical image of the DV organizer is necessary from a morphological point of view since the dorsal and ventral compartments lead, upon development, to the specular dorsal and ventral surfaces of the

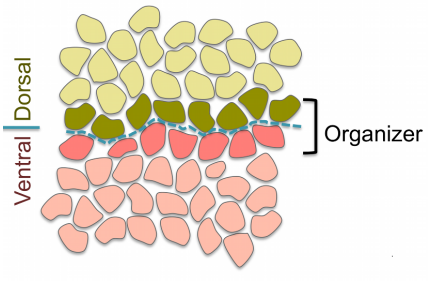

Figure 6: The DV Organizer of the wing imaginal disc.
The DV organizer develops symmetrically with respect to the D and V compartments and acting as a fence prevents cells at the compartments bulk from mixing. The width of the DV organizer population is typically restricted to two cells. The DV boundary (blue dashed line) develops at the middle of the DV organizer and confer distinct mechanical properties to cells.

wing blade in the adult organism. On the other hand, the DV organizer and neighbouring cells give rise to the wing margin.

In the DV case, the gene expression signature of the organizer (Notch activity) is necessary and sufficient for establishing a lineage barrier regardless of the identity of the cell populations. As a consequence, ectopic/displaced activation of the Notch at either dorsal or ventral compartment recreates a functional organizer and, conversely, if Notch signal is blocked, then compartment cells can freely mix. Therefore Notch receptor and its signalling pathway are indispensable elements for the establishment and maintenance of the DV organizer.

Mechanical effects play a central role in the function of the DV organizer. Both actin and myosin accumulate at the junctions of the DV border and their roles are as discussed previously. Further actomyosin based barriers are effective inhibitors of cell mixing in other developmental stages of the Drosophila. This in turns help to keep the straightness and fence-like features of the DV organizer. Other studies also indicate that the consideration of dynamical and morphological factors related with the cell cycle is also required for understanding the stability and robustness of the DV organizer.

4.2 Description of Model

In this section, we are studying the **dynamics and stability** of the DV organizer of the wing imaginal disc of Drosophila as cell proliferation advances by looking at distinctive mechanical properties of cells, differences in cell cycle duration and a well defined cleavage criterion.

The two questions we can ask are: Since cells do not mix, how does the DV organizer robustly deal with the cellular growth in order to prevent cell mixing? Further, how can the organizer be conveniently scaled as the tissue grows since the increase in cell number of the wing imaginal disc is approximately 1000-fold? The vertex model will help us to answer these questions. The model will provide the sufficient ingredients that supply the DV organizer with its features of functionality and robustness during the course of development as cell proliferation advances.

For the cleavage criterion, the angle of division is measured using as a reference an axis perpendicular to the DV boundary such that a null angle corresponds to cells that cleave orthogonally to the DV boundary. The cleavage direction is set perpendicular to the longest axis of symmetry. This is the **Hertwig rule**. Cells of the DV organizer follows a division pattern that is different from cells at the bulk of the compartments, favouring the division plane to be perpendicular to the DV boundary.

As mentioned in Section 3, in this model, the dynamics of each cell vertex depends on the applied forces that derive from mechanical considerations. e.g. cytoskeleton activity. The energy function considered is similar to equation (9). However, there is one additional term. We have instead

$$E(R_i) = \sum_{\alpha} \frac{K_\alpha}{2}(A_\alpha - A_\alpha^{(0)}(t))^2 + \sum_{<i.j>} \Lambda_{ij} l_{ij} + \sum_{\alpha} \frac{\Gamma_\alpha}{2} L_\alpha^2 + \sum_{<i.j>} \frac{\lambda_{ij}}{2} l_{ij}^2 \,. \qquad (13)$$

Dimensionless equation is again used, as shown in equation (10) to (12). For the additional term, we define the dimensionless form of λ_{ij} to be $\bar{\lambda}_{ij} = \frac{\lambda_{ij}}{K_\alpha A_\alpha^{(0)}}$.

The explanations for the 1^{st} to 3^{rd} term are the same as before. For the 1^{st} term however, in addition to the explanation, K_α, which is the elastic energy of cell, is proportional to the Young Modulus due to the difference between the actual cell area A_α and the one that would have due to cytoskeleton structure in the absence of the stresses associated to adhesion and cortical tension, $A_\alpha^{(0)}(t)$. The time dependence of $A_\alpha^{(0)}(t)$ contains the information on the cell cycle and is what drives continuously the system out of equilibrium.

The last 2 terms model further contributions from the mechanical tension associated to the contraction of the actin-myosin cortical ring. The 3^{rd} term is as before. For the 4^{th} term, $\sum_{<i.j>} \frac{\lambda_{ij}}{2} l_{ij}^2$, it is proportional to the squared edge length and in this respect will imitate the mechanical role played by the actin cable at the DV boundary. As for the T1 and T2 processes mentioned in the previous section, they are implemented in the in silico experiments when $l_{ij} < 10^{-1} l^*$, where $l^* = \sqrt{\frac{2A_\alpha^{(0)}}{3\sqrt{3}}}$

is a characteristic edge size defined as the length of a regular hexagonal cell with area $A_\alpha^{(0)}$. Further, the external boundary of tissue is set to be free to move with the same dynamics but with a larger positive line tension, Λ_{ij}, to keep the tissue sufficiently compact, close to a circular shape.

For this paper, I will not be discussing the details of the simulations codes and experiments carried out. I will, instead, state the results in order to answer the questions stated above. The model looks into the wild-type background and the mutant analysis of cells. It reproduces the dynamics and structure of a stable DV organizer that agrees with the available experimental data such as cell division patterns.

4.3 Results

4.3.1 Wild-type Background: Sufficient ingredients for keeping the structure and stability of the growing DV organizer

The initial conditions used in the model assumes a set of 400 regular hexagonal cells with a 2-cells-wide stripe (the fence) specified as the DV organizer. The vertex model includes ingredients that are sufficient to capture a repertoire of experimental observations involving both compartments cells and the DV organizer cells in terms of its structure, stability and dynamics.

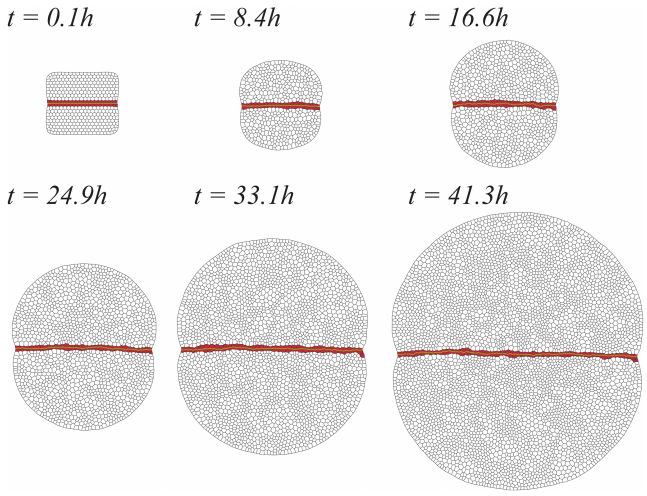

Figure 7: Snapshots of developing in-silico wild-type Wing Disc.
As time evolves the DV organizer (red cells) grows straight maintaining a two-cells width and restrict cells from the compartments bulk (white cells) from mixing.

We see that as time evolves, the DV organizer grows straight, keeping a 2-cell wide population and separating cells of opposite compartment (Figure 7). Further, since the DV organizer is able to cope with the stochastic variability of the cleavage orientation, this reveals its robustness to the scaling process as cell proliferation advances.

4.3.2 Mutant Analysis: Necessary ingredients for keeping the structure and stability of the growing DV organizer

To check to what extent each of the components of the model is indeed required to account for the observed phenomenology mentioned under wild-type background, mutant analysis was carried out. Snapshot of the growth after 7000 dimensionless time units ($\sim$ 40 hours) was used.

To test the fence-like functionality of the DV organizer, the organizer cells are removed completely and the result shows that cells at opposite compartments intermix, generating finger-like pattern (Figure 8A). For the 1st mutant test, the line tension Λ_{ij} between all cells, both bulk and organizer cells are identical. However the differential values for both the line tension and contractility terms that account for the actomyosin cable at the DV boundary is retained. The result then shows that DV organizer is largely disrupted and its fence-like properties disappear (Figure 8B).

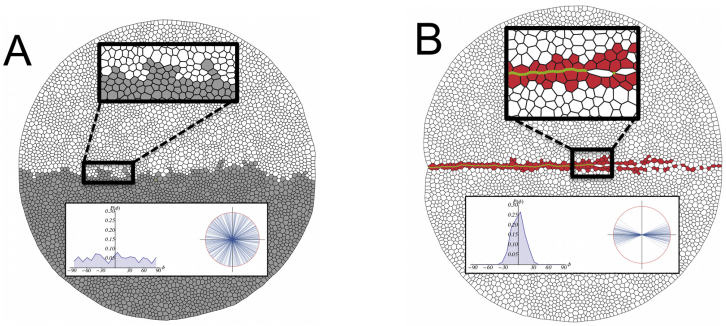

Figure 8: Mutant Analysis. **A**: In the absence of a DV organizer, cells of opposite compartments intermix. **B**: The differential cell adhesion is removed in this simulation and as a result the organizer cannot maintain its stability.

However, if we now have the opposite situation, i.e. maintain the affinities between the organizer and bulk cells but eliminate actomyosin cable by suppressing its distinctive tensile term, the DV organizer is not wiped out as severely as in the previous situation. However, the integrity of the organizer is noticeably weakened as it lacks robustness. The DV boundary becomes less straight and threatens to be ruptured at several points under prolonged proliferation. This shows that when actomyosin cable is removed, the effectiveness of the compartment segregation is reduced (Figure 9C).

Next, we know that orientation of cell divisions determines the shape of developing tissues and organs. So further result shows that if the Hertwig rule is not implemented with respect to the cleavage direction, the DV organizer cannot maintain its stability and becomes easily disrupted. This implies the importance of the role of the Hertwig rule in determining the shape of developing tissues and organs (Figure 9D).

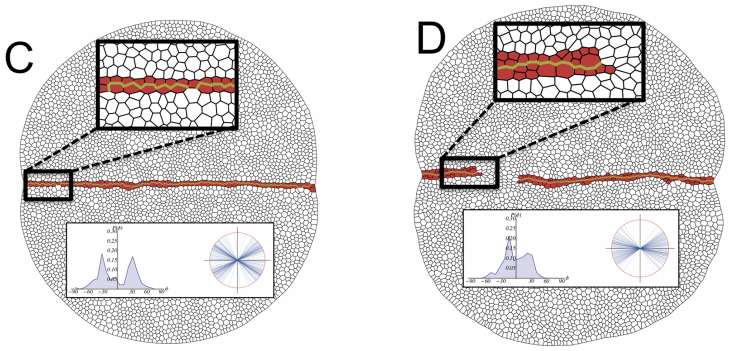

Figure 9: Mutant Analysis. **C**: If the actomyosin cable is removed the width of the organizer is reduced at many locations to one cell and is not robust to perturbations. **D**: A criterion for cell cleavage is required for maintaining the stability of the boundary. In the absence of the Hertwig rule (i.e. cells divide at random orientations), the DV organizer easily breaks, causing cells between compartments to intermingle.

Further, the role played by the distinctive cell cycle durations between organizer and bulk cells is also analysed. A distinctive regulation of the duration of the cell cycle is needed at the DV organizer for maintaining its features and stability. We also need that the cellular mechanical properties and the cleavage direction are coupled by the Hertwig rule.

In addition, the in silico mutant analysis allows the exploration of the role played by the differential affinity of cells at the compartments and the organizer of the actomyosin cable that develops at the DV boundary. Differences in duration are removed and all cells are considered to have the same (mean) lifetime regardless of their lineage. The result shows that the DV boundary becomes very wiggly and the DV organizer becomes wider. (this widening also prevent cells from maintaining its Notch activity) (Figure 10E).

So by using the vertex model, we have shown that distinctive mechanical properties of cells, the differences in cell cycle duration and a cleavage criterion (Hertwig rule) are required for understanding the dynamics, structure and stability of a robust growing DV organizer. Interplay between mechanical effects and the cell growth leads to the functionality and robustness of the growing DV organizer. Further, to

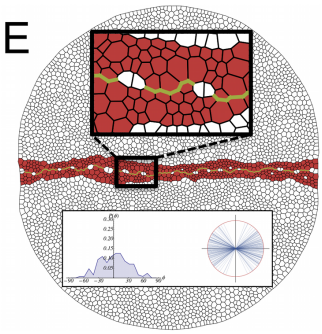

Figure 10: Mutant Analysis. **E**: The duration of the cell cycle is set to be the same in the whole disc. This produces a wiggly boundary and a wide organizer.

sum up, the main differences between the vertex model mentioned in Section 3 as compared to the one described in this section are:

(1) An extra energetic term to account for the asymmetry of actin-myosin expression at different cell edges is included.

(2) The model includes a realistic, stochastic, dynamics of the cell cycle duration, its relation to cell area growth and the implementation of the Hertwig rule with cell-to-cell variability.

(3) Modelling allows for simultaneous cellular growth and a continuous time description that permits to conduct, among others, in silico experiments that provide relevant biochemical information.

(4) Free boundary conditions that do not need to impose a rate for tissue growth is used.

5 Conclusion

The vertex model has been frequently used in conjunction with experimental observations to provide insight into the underlying factors that may drive cell rearrangements. It is used to study the cellular interaction mechanism of rearrangement of cells in developing tissues and was recently used for the analysis of the dorso-ventral segmentation of the growing Drosophila wing.

The model can be modified to include interference by noise. In Figure 2, we have global minimum of energy for the regular network and a local minimum of energy for the soft irregular network. In the presence of noise, we can turn the soft network into a global minimum network. The model can also be applied to other processes such as the study of the dorsal closure mechanism and convergent extension mechanism due to cellular intercalation.

Convergent extension is the process by which the tissue of an embryo is restructured to converge (narrow) along one axis and extend (elongate) along a perpendicular axis by cellular movement. This process plays a crucial role in shaping the body plan during embryogenesis [7]. As for dorsal closure, it takes place midway through Drosophila embryogenesis and is a complex morphogenic process. It is driven by sequential signaling cascades and involves multiple forces which contribute to cell movements and rearrangements as well as to changes in cell shape. During closure, lateral epidermal cells elongate along the dorsoventral axis and subsequently spread dorsally to cover the embryonic dorsal surface. This process represents a well-characterized model for cell sheet morphogenesis during development and wound healing in systems that include vertebrates [6] [8] [9].

The vertex model has its advantages as well as disadvantages as compared with the Cellular Potts model mentioned in the introduction. One of its many advantages is that it uses a computational approach that takes into account the available experimental data for setting a meaningful value of the parameters. This is not the case for the Cellular Potts model.

However, if we would like a model to study the motion of cells by chemotaxis, then Cellular Potts model is favourable. In fact, vertex model was never used. We will need a mesh for putting the chemicals if we would like to use the model for chemotaxis which is a disadvantage. Despite its disadvantages, the vertex model has proven to be successful in many studies to analyse the behaviour of cells. As such, I will continue to work with this model in my summer dissertation and my focus will be on cellular intercalation.

References

[1] Weliky M, Oster G (1990) The mechanical basis of cell rearrangement. I. Epithelial morphogenesis during Fundulus ebipoly. Development 109: 373 – 386.

[2] Honda H, Tanemura M, Nagai T (2004) A three-dimensional vertex dynamics cell model of space-filling polyhedra simulating cell behaviour in a cell aggregate. J Theor Biol 226: 439 – 453.

[3] Farhadifar R, Röper JC, Aigouy B, Eaton S, Jülicher F (2007) The influence of cell mechanics, cell-cell interactions, and proliferation on epithelial packing. Curr Biol 17: 2095 – 2104.

[4] Canela-Xandri O, Sagués F, Casademunt J, Buceta J (2011) Dynamics and Mechanical Stability of the Developing Dorsoventral Organizer of the Wing Imaginal Disc. PLoS Comput Biol 7(9): e1002153. doi:10.1371/journal.pcbi.1002153

[5] Harrison NC, Diez del Corral R, Vasiev B (2011) Coordination of Cell Differentiation and Migration in Mathematical Models of Caudal Embryonic Axis Extension. PLoS ONE 6(7):e22700. doi:10.1371/journal.pone.0022700

[6] Layton A.T, Toyama Y, Yang GQ, Edwards G.S, Kiehart D.P, Venakides S (2009) Drosophila morphogenesis: Tissue force laws and the modeling of dorsal closure. HFSP Journal 3. doi:10.2976/1.3266062

[7] Convergent Extension. Retrieved 8th May 2012. From http://en.wikipedia.org/wiki/Convergent extension

[8] Amnioserosa is required for dorsal closure in Drosophila. Retrieved 8th May 2012. From http://www.mendeley.com/research/amnioserosa-required-dorsal-closure-drosophila/

[9] Dynamic analysis of filopodial interactions during the zippering phase of Drosophila dorsal closure. Retrieved 8th May 2012. From http://dev.biologists.org/content/135/4/621.full

[10] Navier-Stokes Equations. Retrieved 2nd April 2012. From http://en.wikipedia.org/wiki/Navier Stokes equations

A Appendix

A.1 Flattening a cell aggregate under centrifugal force

Exposing the cell aggregate to centrifugal force using equations U_s, U_v, U_z and U_{floor} will flatten the cell aggregate. The force will cause the cells to rotate and spin, making it flat. At first, the cells do not rearrange but subsequent application of centrifugal force rearranges the cells although the shape of the whole cell aggregate does not change.

Once the force is removed (Figure 11), the cells will decrease their flatness, elongate and gradually recover their original shape. Individual cells elongate vertically without rearrangement and their shape depend, not only on the shape of the cell aggregate, but also on the relaxation time. A cell aggregate relaxes as elastic material on short-time scale and as viscous liquids on long-time scale. This is because, the cell aggregate will go back to its original shape under the short time influence of the centrifugal force but not so in the long period of time.

The equation for U_z is

$$U_z = \rho \sum_{\alpha} V_\alpha z_\alpha \,, \tag{14}$$

where U_z is the potential energy induced by centrifugation.

The explanation for the term on the **right-hand side** of equation (14) is as follows:

Body mass m in a centrifugation tube will experience a centrifugal force $F = m\omega^2(R - z)$, where ω is the angular velocity, R is the centrifugation radius at the bottom floor of the tube and z is the distance of the body from the bottom floor.

When $R \ggg z$, $F \approx m\omega^2 R = mg_c$.
($g_c = \omega^2 R$ is the centrifugal acceleration)
$\therefore$ centrifugation gives the body a potential energy, $mg_c z$.

Hence, for a cell α with mass m_α, the potential energy is $m_\alpha g_c z_\alpha$ where z_α is the z-coordinate of the center of mass of the cell. If the mass density of the cells under the centrifugal force is uniform, than the potential energy for cell α can be written as $\rho V_\alpha z_\alpha$. This gives us the potential energy for all cells to be that of equation (14). i.e.

$$U_z = \rho \sum_{\alpha} V_\alpha z_\alpha \,.$$

U_{floor} represent the hindrance of downward motion of cells along the z-axis by the floor below the cell aggregate. In other words, U_{floor} is the constraint from the floor. Cell α moves without restriction when it is above the floor (i.e. $z < 0$), while it produces a large potential energy when it crosses below the floor (i.e. $z > 0$). Since we are working towards minimization of energy, it is important to have this constraint. However, instead of considering U_{floor}, we can replace this term by imposing a boundary condition instead. Nevertheless, U_{floor} is given by the equation

$$U_{\text{floor}} = w_{\text{floor}} \sum_{\alpha} \frac{1}{1 + e^{az_\alpha}} , \tag{15}$$

where w_{floor} is the strength of the potential and a is the slope of the approximated step function (an analytic function is used instead of a step function as we are finding derivative thus we would like to look at a continuous function).

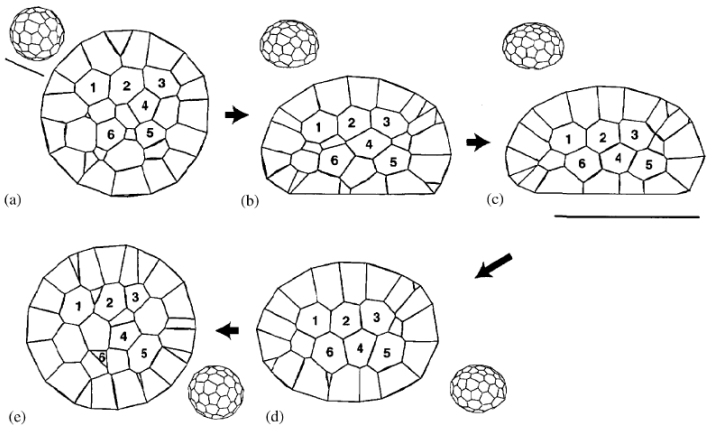

Figure 11: Sections through a cell aggregate during application and removal of centrifugal force. The cell aggregate assumes its original shape after removal of the force.

In analysing the importance of these potential energies, U_s, U_v, U_z and U_{floor}, U_{floor} can be replaced by a boundary condition. U_v is the volume constraint. Although the cells becomes flat under the influence of force, the volume remains fixed (unchanged). Therefore U_v doesn't really play an important role in this model. However, U_s and U_z are two important potential energies which are dependent on each other since U_z represent the pressure of the centrifugal force which effects U_s, the interface energy.

Equations (2), (3), (14) and (15) are transformed using new dimensionless quantities $r_i', \nabla_i' (= \frac{\partial}{\partial r_i'}), S_f', S_m', V_\alpha', V_{std}'$ and z_α' as follows:

$$r_i = r_i' R_0, \Delta_i = \Delta_i'/R_0, S_f = S_f' R_0^2, S_m = S_m' R_0^2, V_\alpha = V_\alpha' R_0^3, V_{std} = V_{std}' R_0^3, z_\alpha = z_\alpha' R_0. \tag{16}$$

After the transformation using equation (16), we get the **equation of motion for the cell aggregate, with centrifugation**, to be

$$\begin{aligned} \frac{dr_i'}{dt'} &= -\nabla_i' \Bigg\{ \sum_f S_f' + \sigma_0 \sum_m S_m' + \kappa' \sum_\alpha (V_\alpha' - V_{std}')^2 \\ &\quad + \rho' \sum_\alpha V_\alpha' z_\alpha' + w_{\text{floor}}' \sum_\alpha \frac{1}{1 + e^{a' z_\alpha'}} \Bigg\}, \end{aligned}$$

where

$$t' = t\sigma/\eta, \sigma_0' = \sigma_0/\sigma, \kappa' = R_0^4 \kappa/\sigma, \rho' = R_0^2 \rho/\sigma, w_{\text{floor}}' = R_0^{-2} w_{\text{floor}}/\sigma, a' = a R_0$$

and omitting the primes ($'$), we get

$$\begin{aligned} \frac{dr_i}{dt} &= -\nabla_i \Bigg\{ \sum_f S_f + \sigma_0 \sum_m S_m + \kappa \sum_\alpha (V_\alpha - 1)^2 \\ &\quad + \rho \sum_\alpha V_\alpha z_\alpha + w_{\text{floor}} \sum_\alpha \frac{1}{1 + e^{a z_\alpha}} \Bigg\}. \end{aligned} \tag{17}$$